INTERNATIONAL JOURNAL FOR NUMERICAL METHODS IN ENGINEERING
Int. J. Numer. Meth. Engng (in press)
Published online in Wiley InterScience (www.interscience.wiley.com). DOI: 10.1002/nme.1985

Numerical examination for degenerate scale problem for ellipse-shaped ring region in BIE

Y. Z. Chen*, †, Z. X. Wang and X. Y. Lin

Division of Engineering Mechanics, Jiangsu University, Zhenjiang, Jiangsu 212013, People's Republic of China

SUMMARY

This paper investigates the degenerate scale problem for an ellipse-shaped ring region in boundary integral equation (BIE). A homogenous integral equation is introduced. The integral equation is reduced to an algebraic equation after discretization. The critical value for the degenerate scale can be obtained from the vanishing condition of a determinant. It is proved that there are two critical values for the degenerate scale, rather than one. This finding is first proposed in the paper. Two particular problems with known solutions are examined numerically. The loadings applied on the exterior boundary may result in a resultant force in the *x*-direction or in the *y*-direction. The improper numerical solutions have been found once the real size approaches the critical value. Two techniques for avoiding the improper solutions are suggested. The techniques depend on the appropriate choice of the used size or adding a constant in a kernel of the integral equation. It is proved that both techniques will give accurate numerical results. Numerical examinations for the problem are emphasized in the paper. Copyright © 2007 John Wiley & Sons, Ltd.

Received 14 June 2006; Revised 28 November 2006; Accepted 13 December 2006

KEY WORDS: boundary integral equation; critical value for the degenerate scale; degenerate scale problem; numerical methods

1. INTRODUCTION

The boundary integral equation (BIE) was widely used in elasticity, and the fundamental concepts of BIE can be found in [1–5]. The early history and qualities of the boundary element method (BEM) were summarized more recently [6]. However, some difficulties for the BIE still exist. The degenerate scale problem in plane elasticity is a particular problem in BIE. If the conventional boundary integral equation (CBIE) is used for an annular region with the vanishing displacements

*Correspondence to: Y. Z. Chen, Division of Engineering Mechanics, Jiangsu University, Zhenjiang, Jiangsu 212013, People's Republic of China.
†E-mail: chens@ujs.edu.cn

Contract/grant sponsor: National Natural Science Foundation of China

along the boundary, in some particular geometry condition the corresponding homogenous integral equation has non-trivial solution for the boundary tractions [7–11]. In fact, if the displacements are vanishing at the boundary of annular region, the stresses must be equal to zero. Therefore, the obtained result seriously violates the basic property of elasticity. In this case, for a real displacement boundary value problem one may obtain an improper solution for the boundary tractions.

It is known that for a given stress field the relevant displacement may be differing by a rigid translation and a rigid rotation. Therefore, the adopted representation of the kernel $U_{ij}^*(\xi, x)$ with a difference of constant (refer to Equations (3), (36)) may significantly influence the property of BIE. This will be a topic in the present study.

It is found that some derivations for the degenerate scale problem in a previous paper were incorrect [7]. In order to get a perfect derivation, some basic equations in the degenerate scale problem in BIE are reexamined.

The degenerate scale problems for simply connected and multiply connected regions of the two-dimensional Laplace equation were studied [12, 13]. It was suggested that from a solution of BEM in the normal scale one can obtain the degenerate scale that is a result of the normal scale multiplied by a factor. It is also proved that the addition of a constant in the fundamental solution, the original degenerate scale is shifting to a new degenerate scale [12]. The degenerate scales for the circular, elliptic, triangular and rectangular boundaries were obtained. Several boundary value problems from torsion bar were solved based on the suggested BEM [12].

In this paper, the degenerate scale problem for an ellipse-shaped ring region in BIE is considered. In the formulation, the kernel $U_{ij}^*(\xi, x)$, or the displacement for the fundamental field, is expressed in a usual form. Meantime, a particular dimension 'a' which causes a non-trivial solution to the relevant homogenous integral equation is defined as the critical value for the degenerate scale. Clearly, this solution cannot be obtained in a closed form. Further, the integral equation can be reduced to an algebraic equation after discretization. In this case, one will obtain the critical value for the degenerate scale from the vanishing condition of a determinant. It is proved from computed results that there are two critical values for the degenerate scale (λ_1 and λ_2) in the present case. This finding is first proposed in the present study.

In addition to finding the critical value for the degenerate scale, two particular problems with known solutions are taken as examples for numerical examination. In the problem, some loadings are applied along the exterior and interior boundaries, and the whole loadings are in equilibrium. The loadings applied on the exterior boundary or on the interior boundary result in a resultant force in the x-direction or in the y-direction. After substituting the known displacements in the BIE, the boundary tractions are evaluated from the BIE. The obtained numerical results are compared with those from the exact solution, and the relevant deviations are computed. It is found that if the adopted size differs from the critical value for the degenerate scale by a rather small value, saying, 0.00002 ($=0.0013\%$ of the critical value), the computed results are incorrect. Meantime, if the adopted size differs from the critical value for the degenerate scale by more than 10%, the computed results coincide with those from the exact solution. The details will be introduced later.

Two techniques for avoiding the improper solution are suggested. In the first technique, the used size 'a' should not be too near to two critical values (λ_1 and λ_2). In the second technique, one needs to adjust the constant involved in the kernel $U_{ij}^*(\xi, x)$. In this case, the two critical values (λ_1 and λ_2) will be considerably reduced (or evaluated). Therefore, the used size 'a' will differ from two critical values (λ_1 and λ_2) significantly. It is proved from computation that both techniques will give accurate numerical results. Numerical computation is highlighted and emphasized in this paper.

DOI: 10.1002/nme

2. FUNDAMENTAL ASPECTS OF THE DEGENERATE SCALE PROBLEM IN BIE

The fundamental aspects of the degenerate scale problem for an annular region in BIE are introduced. It is found that some derivations for this problem may be incorrect [7]. Therefore, a correct formulation for this problem is carried out. Formulation of the degenerate scale problem for the ellipse-shaped ring region in BIE is addressed. Numerical evaluations for the critical values for the degenerate scale for the annular region and the ellipse-shaped ring region are carried out.

2.1. Formulation of the degenerate scale problem for the ellipse-shaped ring region in BIE

Without losing generality, we introduce the BIE for the ellipse-shaped ring region with two ellipses (Figure 1). The exterior ellipse has two half-axes (a, b) and the interior ellipse has two half-axes (c, d). The relation $c/a = d/b$ is generally assumed. The field point '$\xi(\xi_1, \xi_2)$' is assumed on the exterior boundary (B_0) or the interior boundary (B_1), and the integration is performed for the source point '$x(x_1, x_2)$'. For the plane strain case, the suggested BIE can be written as follows [3]:

$$\frac{1}{2}u_i(\xi) + \int_{B_0+B_1} P^*_{ij}(\xi, x)u_j(x)\,\mathrm{d}s(x) = \int_{B_0+B_1} U^*_{ij}(\xi, x)p_j(x)\,\mathrm{d}s(x) \quad (\text{for } i = 1, 2,\ \xi \in B_0 \text{ or } \xi \in B_1) \tag{1}$$

where the kernel $P^*_{ij}(\xi, x)$ and $U^*_{ij}(\xi, x)$ are defined by [3]

$$P^*_{ij}(\xi, x) = -\frac{1}{4\pi(1-\nu)}\frac{1}{r}\{(r_{,1}n_1+r_{,2}n_2)((1-2\nu)\delta_{ij}+2r_{,i}r_{,j})+(1-2\nu)(n_i r_{,j}-n_j r_{,i})\} \tag{2}$$

$$U^*_{ij}(\xi, x) = H\{(3-4\nu)\,\ln(r)\delta_{ij} - r_{,i}r_{,j}\} \quad \text{with } H = \frac{-1}{8\pi(1-\nu)G} \tag{3}$$

G is the shear modulus of elasticity, ν is the Poisson ratio.

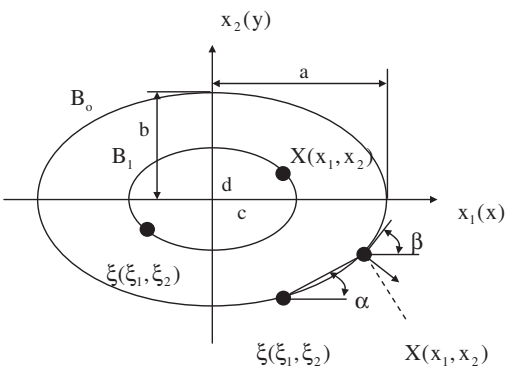

Figure 1. Boundary value problem for an ellipse-shaped ring region.

DOI: 10.1002/nme

In Equations (2) and (3), the Kronecker deltas δ_{ij} is defined as, $\delta_{ij}=1$ for $i=j$, $\delta_{ij}=0$ for $i\neq j$, and

$$r=\sqrt{(x_1-\xi_1)^2+(x_2-\xi_2)^2},\quad r_{,1}=\frac{x_1-\xi_1}{r}=\cos\alpha,\quad r_{,2}=\frac{x_2-\xi_2}{r}=\sin\alpha$$
$$n_1=\sin\beta,\quad n_2=-\cos\beta\quad\text{(for a point on the exterior circle)} \tag{4}$$

where the angles 'α' and 'β' are indicated in Figure 1.

Note that some researchers wrote the kernel in the form $U^*_{ij}(\xi,x)=H\{(3-4\nu)\ln(r/a_d)\delta_{ij}-r_{,i}r_{,j}\}$ [7]. It is found that it is also a convenient way to write the kernel in the form of Equation (3).

Two types of particular problems, the problem 'A' and problem 'B', are introduced. In the problem 'A', the boundary tractions $p_j(x)$ are known beforehand. From those known boundary tractions, we can define

$$g_i(\xi)=\int_{B_0+B_1}U^*_{ij}(\xi,x)p_j(x)\,\mathrm{d}s(x)\quad(\text{for } i=1,2,\ \xi\in B_0 \text{ or } \xi\in B_1) \tag{5}$$

Therefore, A BIE for $u_j(x)$ as unknowns can be formulated

$$\frac{1}{2}u_i(\xi)+\int_{B_0+B_1}P^*_{ij}(\xi,x)u_j(x)\,\mathrm{d}s(x)=g_i(\xi)\quad(\text{for } i=1,2,\ \xi\in B_0 \text{ or } \xi\in B_1) \tag{6}$$

Sometimes, the problem 'A' is called the traction boundary value problem, which is similar to the Neumann problem of Laplace equation.

In the problem 'B', the boundary displacements $u_j(x)$ are known beforehand. From those known boundary displacements, we can define

$$h_i(\xi)=\frac{1}{2}u_i(\xi)+\int_{B_0+B_1}P^*_{ij}(\xi,x)u_j(x)\,\mathrm{d}s(x)\quad(\text{for } i=1,2,\ \xi\in B_0 \text{ or } \xi\in B_1) \tag{7}$$

Therefore, A BIE for $p_j(x)$ as unknowns can be formulated

$$\int_{B_0+B_1}U^*_{ij}(\xi,x)p_j(x)\,\mathrm{d}s(x)=h_i(\xi)\quad(\text{for } i=1,2,\ \xi\in B_0 \text{ or } \xi\in B_1) \tag{8}$$

Sometimes, the problem 'B' is called the displacement boundary value problem, which is similar to the Dirichlet problem of Laplace equation.

The degenerate scale problem is a particular problem in the problem 'B'. Without losing generality, it is assumed that the ratios b/a and c/a are given beforehand. It is preferable to write the kernel in Equation (8) in the form of $U^*_{ij}(\xi,x,a)$. The relevant homogeneous equation to Equation (8) is introduced

$$\int_{B_0+B_1}U^*_{ij}(\xi,x,a)p_j(x)\,\mathrm{d}s(x)=0\quad(\text{for } i=1,2,\ \xi\in B_0 \text{ or } \xi\in B_1) \tag{9}$$

In some particular values of 'a', Equation (9) may have a non-trivial solution (note that $p_j(x)=0$ is a trivial solution). Those particular values for 'a' are called the critical value for the degenerate scale, hereafter.

DOI: 10.1002/nme

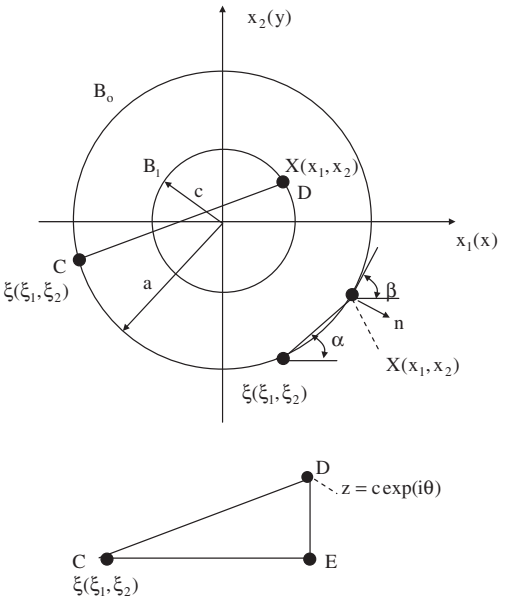

Figure 2. Boundary value problem for an annular region.

Unfortunately, only the critical value for the generate scale for the annular region $b/a = 1$ was obtained in a closed form previously. However, some derivations were incorrect in [7]. Therefore, a correct derivation is introduced in the following paragraph. Secondly, for the general case of $b/a \neq 1$, a detailed numerical evaluation for the critical value for the degenerate scale is also carried out below.

2.2. Formulation of the degenerate scale problem for an annular region in BIE

The solution for the degenerate scale problem for an annular region ($b/a = 1$) was studied previously (Figure 2). However, some derivations were incorrect in [7]. Therefore, a correct derivation is introduced below.

We may introduce two integrals as follows:

$$J_i = \int_{B_0+B_1} U_{ij}^*(\xi, x, a)\, p_j(x)\, \mathrm{d}s(x) \quad (i = 1, 2) \tag{10}$$

and intend to find a non-trivial solution for the following homogeneous integral equation:

$$J_i = \int_{B_0+B_1} U_{ij}^*(\xi, x, a)\, p_j(x)\, \mathrm{d}s(x) = 0 \quad (i = 1, 2) \quad \text{(same as Equation (9))} \tag{10a}$$

Clearly, $p_j = 0$ $(j = 1, 2)$ is a trivial solution and it is of no meaning in the present study.

DOI: 10.1002/nme

If substituting $p_1=g_0$ and $p_2=0$ (for $(x(x_1, x_2)\in B_0)$) and $p_1=g_1$ and $p_2=0$ (for $(x(x_1, x_2)\in B_1)$) into Equation (10) we will find

$$J_1 = H\pi a g_0[2(3-4\nu)\ln a - 1] + H\pi c g_1[2(3-4\nu)\ln a - (1+\cos 2\beta_0 - \delta^2\cos 2\beta_0)] \quad (\text{for } \xi = a\exp(\mathrm{i}\beta_0)\in B_0) \tag{11}$$

$$J_1 = H\pi a g_0[2(3-4\nu)\ln a - 1] + H\pi c g_1[2(3-4\nu)\ln c - 1] \quad (\text{for } \xi = c\exp(\mathrm{i}\beta_1)\in B_1) \tag{12}$$

$$J_2 = H\pi c g_1[-(1-\delta^2)\sin 2\beta_0] \quad (\text{for } \xi = a\exp(\mathrm{i}\beta_0)\in B_0) \tag{13}$$

$$J_2 = 0 \quad (\text{for } \xi = c\exp(\mathrm{i}\beta_1)\in B_1) \tag{14}$$

where $\delta = c/a$ (Figure 2).

It is found that the counterparts for Equations (11) and (12) were wrongly derived in Equations (11), (12) of [7]. Also, the conclusion based on the second equation of Equation (13) of [7] is incorrect. For the correct derivation of the second term in Equation (11), one can refer to the Appendix. In this paper, we have examined the correctness of Equations (11)–(14) by numerical computation.

Form Equations (11) and (12), it is suitable to find a particular value for 'a', which satisfies

$$2(3-4\nu)\ln a - 1 = 0 \tag{15}$$

The solution of Equation (15) is found to be

$$a = \gamma_{\mathrm{d}}, \quad \text{where } \gamma_{\mathrm{d}} = \exp[1/2(3-4\nu)] \tag{16}$$

The value 'a' (now $a=\gamma_{\mathrm{d}}$) is called the critical value for the degenerate scale hereafter. If $\nu=0.3$ we have $\gamma_{\mathrm{d}}=1.32019$.

From the above-mentioned results shown by Equations (11)–(14), the following conclusion is deduced. If condition (16) (or $a=\gamma_{\mathrm{d}}$) is satisfied, $p_1=g_0$ (g_0—any constant value) $p_2=0$ (for $(x(x_1, x_2)\in B_0)$) and $p_1=g_1=0$, $p_2=0$ (for $(x(x_1, x_2)\in B_1)$) is a non-trivial solution for the integral equation (9) or (10a).

2.3. Numerical examination for the critical value for degenerate scale for the annular region

To confirm the above-mentioned result, the critical value for the degenerate scale 'a' is evaluated numerically. For the annular region, we have $b/a=1$. In the numerical examination, two circles having a ratio $c/a=0.5$ are divided into 60 intervals, and $\nu=0.3$ is assumed (Figure 2). The constant displacement and traction are assumed for each interval. After making discretization, Equation (9) can be reduced to

$$\sum_{n=1}^{M} U_{mn}\, p_n = 0 \quad (m=1, 2, \ldots, M) \tag{17}$$

where the matrix 'U_{mn}' $(m, n=1, \ldots, M)$ is derived from the kernel function '$U^*_{ij}(\xi, x, a)$', and 'p_n' denotes the loading vector that is assumed on the nodes. Equation (17) may be written in a

DOI: 10.1002/nme

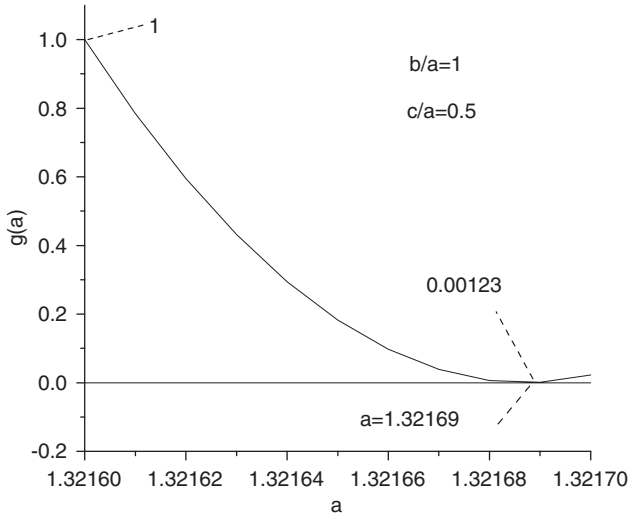

Figure 3. Computed values of the function $g(a)$ for the range $a \approx r_d$ under the condition $b/a = 1$.

matrix form as follows:

$$\mathbf{U}\mathbf{p} = 0 \tag{18a}$$

The algebraic equation (18a) can be expressed in the form

$$\mathbf{U}\mathbf{p} = \lambda\mathbf{p} \quad \text{(with the scalar } \lambda = 0\text{)} \tag{18b}$$

Therefore, the problem for finding non-trivial solution for the vector $\mathbf{p}$ from Equation (18a) is called the zero eigenvalue problem in literature.

In computation, we can assume a lot of values for 'a' ($a_1 \leqslant a \leqslant a_2$) and find the value of det($\mathbf{U}$). The computed result is expressed as

$$g(a) = \det(\mathbf{U})/h(a_1), \quad \text{where } h(a) = \det(\mathbf{U}) \quad (a_1 \leqslant a \leqslant a_2) \tag{19}$$

The computed $g(a)(1.32160 \leqslant a \leqslant 1.32170)$ is plotted in Figure 3. From Figure 3 we find that a minimum for $g(a)$ is reached at $a = 1.32169$. This value is defined as the critical value for the degenerate scale. On the other hand, substituting $v = 0.3$ into Equation (16) yields $a_{\text{exact}} = 1.32019$. It is found that the deviation of the numerical result for 'a' from the exact one is minor.

One point needs to be explained in detail. Theoretically, if Equation (17) has a non-trivial solution, det($\mathbf{U}$) must be equal to zero. However, in the present computation, all the values of det($\mathbf{U}$) within the investigated range ($1.32160 \leqslant a \leqslant 1.32170$) take a positive value. In this case, the criterion that $g(a)$ reaches a relatively small value is used to find the critical value for 'a'. In fact, from the computed results we have

$$(g(a)|_{a=1.32169})/(g(a)|_{a=1.32160}) = (0.00123)/(1.00000) \tag{20}$$

On the other hand, we have examined the critical values for the degenerate scale for four cases $c/a = 0.2, 0.4, 0.6$ and 0.8. It is found that the obtained critical values coincide with the value

DOI: 10.1002/nme

obtained in the $c/a = 0.5$ case. In fact, the theoretical result shown by Equation (16) does not depend on the ratio c/a.

2.4. Numerical examination for the critical value for degenerate scale for the ellipse-shaped ring region

In the case of a ellipse-shaped ring region, we can evaluate the critical value for the degenerate scale in a similar way (Figure 1). First, we can define the following function in an interval $a_1 \leqslant a \leqslant a_2$:

$$g(a) = \det(\mathbf{U})/h(a_1), \quad \text{where } h(a) = \det(\mathbf{U}) \quad (a_1 \leqslant a \leqslant a_2) \tag{19}$$

The critical value for size 'a' will be obtained from the following condition:

$$g(a) = 0 \tag{21}$$

Two particular cases should be particularly emphasized. If the size 'a' is not equal to some particular values which are called the critical values below (λ_1 and λ_2), the determinant for the matrix U (or $\det(U)$) is not equal to zero. In this case, we have a solution $p_m = 0$ ($m = 1, 2, \ldots, M$) from Equation (17). On the contrary, one can find a size 'a' such that the determinant for the matrix U (or $\det(U)$) is equal to zero. Those particular values for the size 'a' are called the critical values below (λ_1 and λ_2). In this case, we have a non-trivial solution from Equation (17), or at least one of p_m ($m = 1, 2, \ldots, M$) is not equal to zero. From knowledge of linear algebra and matrix theory, the matrix U is singular or it is rank deficient. Therefore, when the size 'a' is equal to the critical values, the following statements are equivalent; (1) the $\det(U) = 0$, or the determinant of matrix U is equal to zero, (2) the matrix U is singular or it is rank deficient.

We take the case of $b/a = 0.98$ with $c/a = 0.5$ as an example. The computation is performed within the range $1.330 \leqslant a \leqslant 1.340$. The computed function $g(a)$ ($1.330 \leqslant a \leqslant 1.340$) is plotted in Figure 4. From the plotted results, we can find two zeros of the function $g(a)$

$$a = \lambda_1 \quad (\lambda_1 = 1.3312) \tag{22}$$

$$a = \lambda_2 \quad (\lambda_2 = 1.3387, \lambda_2 > \lambda_1) \tag{23}$$

In addition, the critical values are evaluated for many cases for $b/a = 0.1, 0.2, \ldots, 1.0$, and $b/a = 0.90, 0.91, \ldots, 0.99, 1.00$. The calculated results are shown in Figure 5 and Table I. The following results are significant from the computed results. Computed results prove that critical values do not depend on the ratio c/a.

Except for the case of $b/a = 1$, there are two critical values for the degenerate scale $a = \lambda_1$ and λ_2. This result is first finding of this paper. However, when $a/b \to 1$ or $a/b = 1$, the elliptic ring region is reduced to a circular ring region. For the circular ring region, the symmetric conditions for two axes x and y are the same. In this case, when $a/b = 1$ two critical values must merge into one size $a = \lambda_1 = \lambda_2 = 1.32168$ (see Table I). This tendency can be found from Figure 5 and Table I (refer to three cases $b/a = 0.98$, 0.99 and 1). Alternatively speaking, this must be the case of double roots for equation $g(a) = 0$ if $a/b = 1$.

Also, some researchers suggested an equation for the critical value [8]. After the 'a' value (for the annular region) in Equation (16) is replaced by $(a + b)/2$ (for the ellipse-shaped ring region),

DOI: 10.1002/nme

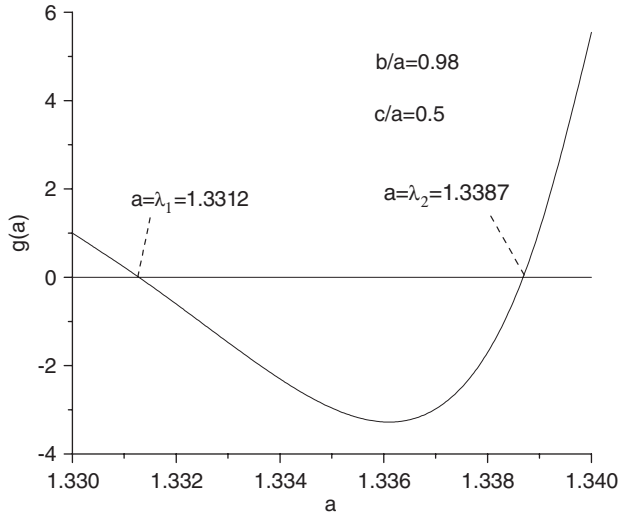

Figure 4. Computed values of the function $g(a)$ within the range $1.33 \leqslant a \leqslant 1.34$ under the condition $b/a = 0.98$.

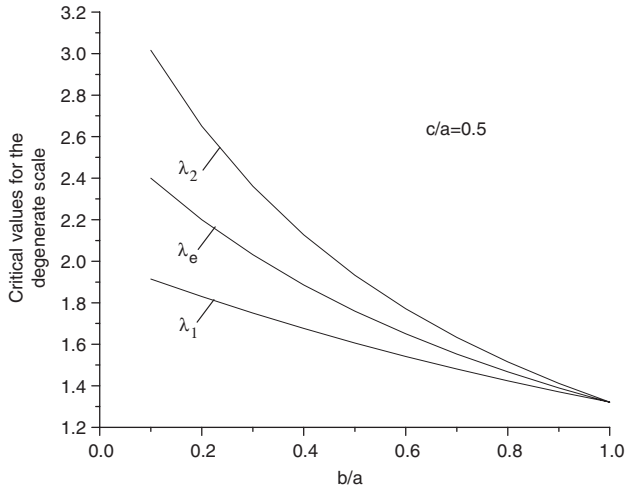

Figure 5. Computed values of two critical values $a = \lambda_1$ and $a = \lambda_2$ within the range $0.1 \leqslant b/a \leqslant 1.0$.

it follows

$$(a+b)/2 = \gamma_{\mathrm{d}} \quad \text{or} \quad a = \lambda_{\mathrm{e}} \quad \text{where } \lambda_{\mathrm{e}} = \frac{2a}{a+b}\gamma_{\mathrm{d}} \tag{24}$$

This estimation ($a = \lambda_{\mathrm{e}}$) for the critical value is also plotted in Figure 5.

DOI: 10.1002/nme

Table I. Computed values of two critical values for the degenerate scale $a=\lambda_1$ and λ_2 within the ranges $0.1\leqslant b/a\leqslant 1.0$ and $0.9\leqslant b/a\leqslant 1.0$.

	b/a									
	0.1	0.2	0.3	0.4	0.5	0.6	0.7	0.8	0.9	1.0
λ_1	1.91454	1.83042	1.75088	1.67621	1.60640	1.54127	1.48054	1.42390	1.37015	1.32168
λ_2	3.01622	2.65095	2.36148	2.12682	1.93321	1.77091	1.63304	1.51457	1.41173	1.32168
λ_e	2.40035	2.20032	2.03106	1.88599	1.76025	1.65024	1.55316	1.46688	1.38967	1.32019
	b/a									
	0.90	0.91	0.92	0.93	0.94	0.95	0.96	0.97	0.98	0.99	1.00
λ_1	1.37105	1.36590	1.36090	1.35580	1.35090	1.34590	1.34100	1.33610	1.33120	1.32640	1.32168
λ_2	1.41173	1.40210	1.39270	1.38340	1.37430	1.36520	1.35630	1.34750	1.33870	1.33010	1.32168
λ_e	1.38967	1.38240	1.37520	1.36807	1.36102	1.35404	1.34713	1.34029	1.33353	1.32682	1.32019

3. NUMERICAL EXAMINATION FOR THE DEGENERATE SCALE PROBLEM

The problem '*A*' defined by Equation (6) was computed in this study. Since there was nothing wrong in computation, computed results for the problem will not be mentioned. The numerical examination is devoted to the problem '*B*' defined by Equation (8).

Two particular problems with the known solutions are taken as an example for the numerical examination. In the problem, some loadings are applied the exterior and interior boundaries, and the whole loadings are in equilibrium. The loadings applied on the exterior boundary or on the interior boundary result in a resultant force in x- or in y-direction. After substituting the known displacements in Equation (7), the boundary tractions are evaluated from the BIE, or from the integral equation (8). The obtained numerical results are compared with those from the exact solution, and the relevant deviations are evaluated.

3.1. Some equations in plane elasticity

The following analysis may use the complex variable function method in plane elasticity [14]. In the method, the stresses $(\sigma_x, \sigma_y, \sigma_{xy})$, the resultant forces (X, Y) and the displacements (u, v) are expressed in terms of two complex potentials $\phi(z)$ and $\psi(z)$ such that

$$\begin{aligned} \sigma_x+\sigma_y &= 4\,\mathrm{Re}\,\phi'(z) \\ \sigma_y-\sigma_x+2\mathrm{i}\sigma_{xy} &= 2[\overline{z}\phi''(z)+\psi'(z)] \end{aligned} \tag{25}$$

$$f=-Y+\mathrm{i}X=\phi(z)+z\overline{\phi'(z)}+\overline{\psi(z)} \tag{26}$$

$$2G(u+\mathrm{i}v)=\kappa\phi(z)-z\overline{\phi'(z)}-\overline{\psi(z)} \tag{27}$$

where $z=x+\mathrm{i}y$ denotes complex variable, G is the shear modulus of elasticity, $\kappa=(3-v)/(1+v)$ is for the plane stress problem, $\kappa=3-4v$ is for the plane strain problem, and v is the Poisson ratio. In the present study, the plane strain condition is assumed thoroughly.

DOI: 10.1002/nme

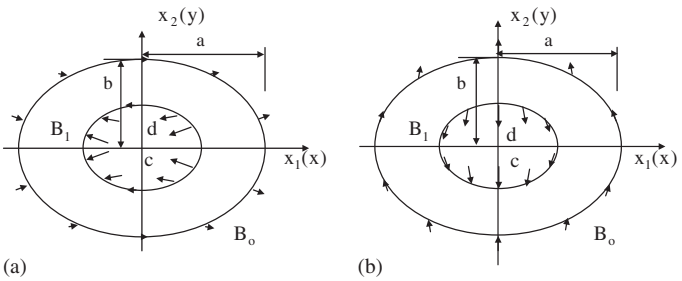

Figure 6. (a) Loading condition for the ellipse-shaped ring region with a resultant force in the x-direction along the exterior or interior boundary and (b) loading condition for the ellipse-shaped ring region with a resultant force in the y-direction along the exterior or interior boundary.

3.2. Numerical examination by a displacement boundary value problem, the problem 'B'

The above-mentioned results for the degenerate scale problem can be examined by the following concrete example. In the example, we propose the following complex potentials:

$$\phi(z) = F \ln z, \quad \psi(z) = -\kappa F \ln z \tag{28}$$

where 'F' is a loading that has a dimension of force. Therefore, from Equations (25)–(27), the stresses and the displacements can be evaluated

$$\sigma_x + \sigma_y = 4F \operatorname{Re} \frac{1}{z}, \quad \sigma_y - \sigma_x + 2\mathrm{i}\sigma_{xy} = -2F\left(\frac{\bar{z}}{z^2} + \frac{\kappa}{z}\right) \tag{29}$$

$$2G(u + \mathrm{i}v) = F\left(2\kappa \ln |z| - \frac{z}{\bar{z}}\right) \tag{30}$$

Meantime, from Equation (26) the amount of the resultant force in the x-direction applied on the interior boundary or on the exterior boundary will be $2\pi(\kappa+1)F$. The relevant loading condition is shown in Figure 6(a).

In the numerical examination, the BIE takes the form of Equation (8). Once the displacements $u_j(x)$ $(j = 1, 2)$ obtained from the exact solution are substituted into Equation (7), the $f_i(\xi)$ $(i = 1, 2)$ are obtainable, which in turn become the right-hand term of the BIE Equation (8).

In computation, the exterior ellipse has the two half-axes 'a' and 'b' with the ratio $b/a = 0.5$. Two similar ellipses having a ratio $c/a = 0.5$ are divided into 60 intervals and the condition $b/a = d/c$ is assumed (Figure 6(a)). Constant displacement and traction are assumed for each interval. Standard numerical technique is used to solve the BIE shown by Equation (8) numerically.

As mentioned previously, there are two critical values $a = \lambda_1 = 1.60640$ and $a = \lambda_2 = 1.93321$ (for $b/a = 0.5$ case), which are shown in Table I. The computed results for tractions are expressed as follows:

$$p_1 = f_x(\theta)\frac{\pi(\kappa+1)F}{a}, \quad p_2 = f_y(\theta)\frac{\pi(\kappa+1)F}{a}$$

$$\text{(for tractions on the exterior boundary } x = a\cos\theta,\ y = b\sin\theta) \tag{31}$$

DOI: 10.1002/nme

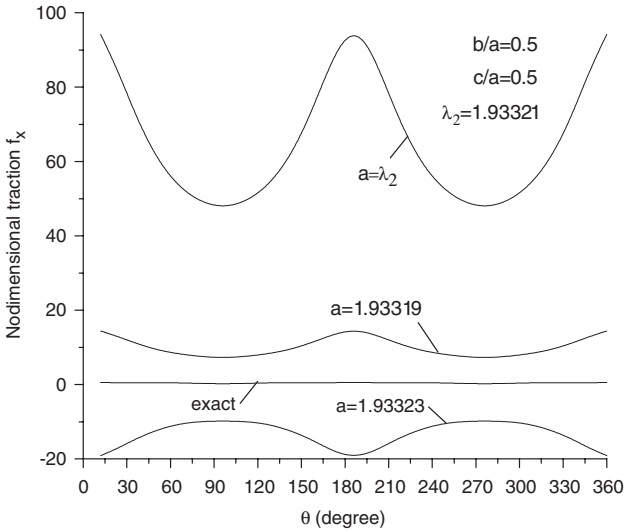

Figure 7. Non-dimensional boundary tractions $f_x(\theta)$ on the exterior boundary in the first example, for $a=\lambda_2-\varepsilon$, $a=\lambda_2$ and $a=\lambda_2+\varepsilon$ cases ($\lambda_2=1.93321$, $\varepsilon=0.00002$) under the condition $b/a=0.5$ and $c/a=0.5$ (see Figures 1, 6(a) and Equation (31)).

$$p_1=g_x(\theta)\frac{\pi(\kappa+1)F}{a},\quad p_2=g_y(\theta)\frac{\pi(\kappa+1)F}{a}$$
$$\text{(for tractions on the interior boundary } x=c\cos\theta,\ \ y=d\sin\theta) \tag{32}$$

For the mentioned loading case, computations for five cases, $a=\lambda_2-0.00002$, $a=\lambda_2$, $a=\lambda_2+0.00002$, $a=0.9\lambda_2$, and $a=1.1\lambda_2$ ($\lambda_2=1.93321$) are performed. The computed results for $f_x(\theta)$, $f_y(\theta)$, $g_x(\theta)$ and $g_y(\theta)$ are plotted in Figures 7–12. For comparison, the exact results from Equations (25)–(30) are also shown in the figures.

The most significant feature of the degenerate scale problem can be seen from Figures 7 and 8. In fact, the exact values for $f_x(\theta)$ are varying within the ranges $0.182\leqslant f_x(\theta)\leqslant 0.540$ (see Figure 8). However, if $a=\lambda_2$ is adopted, we have $f_x(\theta)|_{\theta=12^\circ}=94.210$. Therefore, the obtained results are incorrect in general if $a=\lambda_2$ is adopted. In addition, if $a=0.9\lambda_2$ or $a=1.1\lambda_2$ is adopted, the error for $f_x(\theta)$ from the exact solution is very small, as shown in Figure 8. From Figures 9–12, it is seen that the dependence of the functions $f_y(\theta)$, $g_x(\theta)$ and $g_y(\theta)$ to the used size is minor. It is interesting to point out that only the function $f_x(\theta)$ (i.e. the p_1 component along the exterior boundary) has a unstable numerical result when $a\approx\lambda_2$ (refer to Figure 7).

For the mentioned loading case, computations are also made for five cases, $a=\lambda_1-0.00002$, $a=\lambda_1$, $a=\lambda_1+0.00002$, $a=0.9\lambda_1$, and $a=1.1\lambda_1$ ($\lambda_1=1.60640$) are performed. In the computations, improper results are not found.

The situation in the first example is similar to the case discussed in the problem of the annular region. From the above-mentioned results shown by Figures 7–12, the following property may be found. If the condition $a=\lambda_2$ is satisfied, $p_1=g_0$ (g_0—any constant value) $p_2=0$ (for $(x(x_1,x_2)\in B_0)$) and $p_1=g_1=0$, $p_2=0$ (for $(x(x_1,x_2)\in B_1)$) is a non-trivial solution for the homogeneous integral equation (9).

DOI: 10.1002/nme

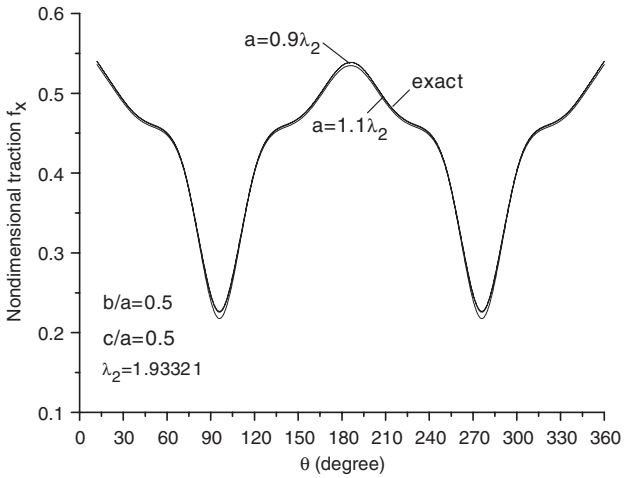

Figure 8. Non-dimensional boundary tractions $f_x(\theta)$ on the exterior boundary in the first example, for $a=0.9\lambda_2$ and $a=1.1\lambda_2$ cases ($\lambda_2=1.93321$) under the condition $b/a=0.5$ and $c/a=0.5$ (see Figures 1, 6(a) and Equation (31)).

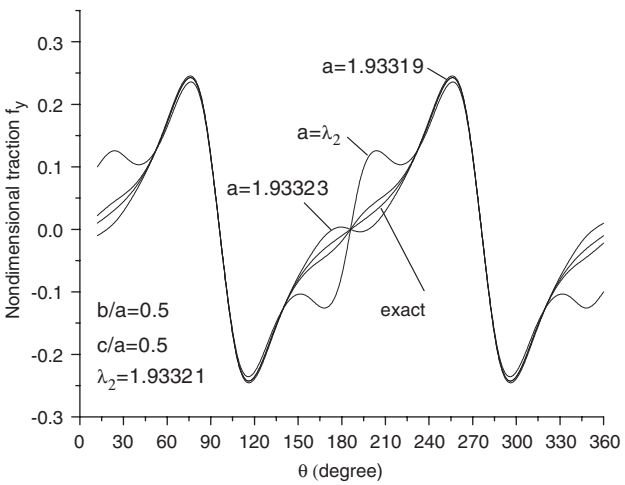

Figure 9. Non-dimensional boundary tractions $f_y(\theta)$ on the exterior boundary in the first example, for $a=\lambda_2-\varepsilon$, $a=\lambda_2$, and $a=\lambda_2+\varepsilon$ cases ($\lambda_2=1.93321$, $\varepsilon=0.00002$) under the condition $b/a=0.5$ and $c/a=0.5$ (see Figures 1, 6(a) and Equation (31)).

However, we soon find that the other critical value $a=\lambda_1$ will also give improper results in the following example. In the example, we propose the following complex potentials:

$$\phi(z)=\mathrm{i}F\ln z, \quad \psi(z)=\mathrm{i}\kappa F\ln z \tag{33}$$

DOI: 10.1002/nme

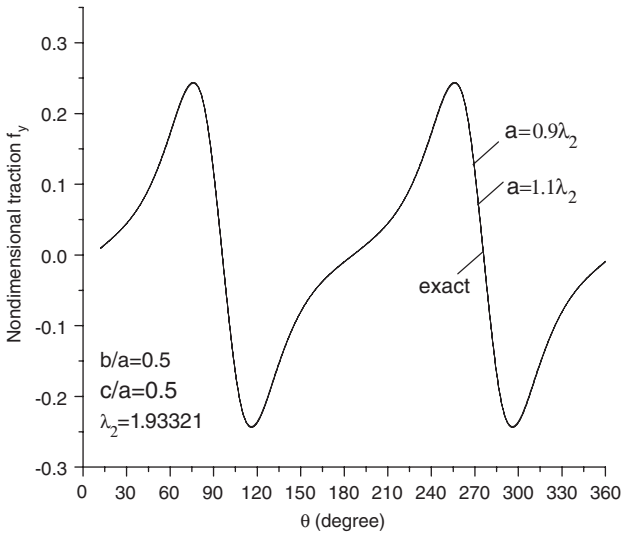

Figure 10. Non-dimensional boundary tractions $f_y(\theta)$ on the exterior boundary in the first example, for $a=0.9\lambda_2$ and $a=1.1\lambda_2$ cases ($\lambda_2=1.93321$) under the condition $b/a=0.5$ and $c/a=0.5$ (see Figures 1, 6(a) and Equation (31)).

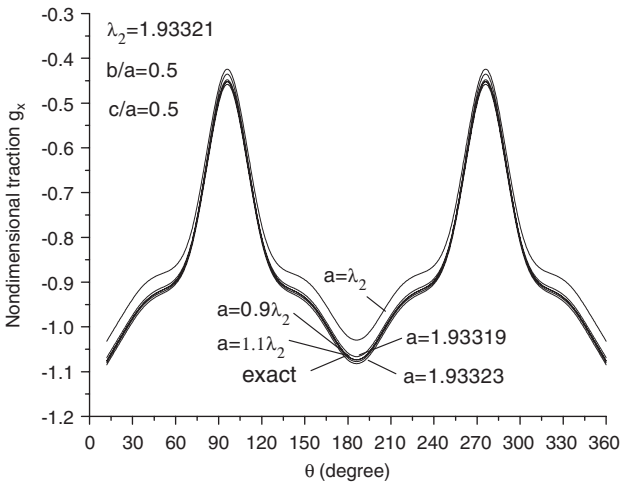

Figure 11. Non-dimensional boundary tractions $g_x(\theta)$ on the interior boundary in the first example, for $a=\lambda_2-\varepsilon$, $a=\lambda_2$, $a=\lambda_2+\varepsilon$, $a=0.9\lambda_2$ and $a=1.1\lambda_2$ cases ($\lambda_2=1.93321, \varepsilon=0.00002$) under the condition $b/a=0.5$ and $c/a=0.5$ (see Figures 1, 6(a) and Equation (32)).

where 'F' is a loading that has a dimension of force. Therefore, from Equations (25)–(27), the stresses and the displacements can be evaluated

$$\sigma_x+\sigma_y=4F\,\mathrm{Re}\,\frac{\mathrm{i}}{z},\quad \sigma_y-\sigma_x+2\mathrm{i}\sigma_{xy}=2\mathrm{i}F\left(-\frac{\overline{z}}{z^2}+\frac{\kappa}{z}\right) \tag{34}$$

DOI: 10.1002/nme

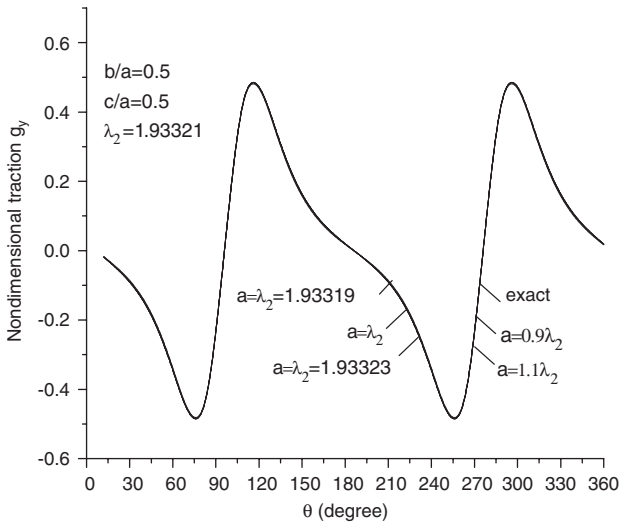

Figure 12. Non-dimensional boundary tractions $g_y(\theta)$ on the interior boundary in the first example, for $a=\lambda_2-\varepsilon$, $a=\lambda_2$, $a=\lambda_2+\varepsilon$, $a=0.9\lambda_2$ and $a=1.1\lambda_2$ cases ($\lambda_2=1.93321$, $\varepsilon=0.00002$) under the condition $b/a=0.5$ and $c/a=0.5$ (see Figures 1, 6(a) and Equation (32)).

$$2G(u+\mathrm{i}v)=\mathrm{i}F\left(2\kappa\ln|z|+\frac{z}{\overline{z}}\right) \tag{35}$$

Meantime, from Equation (26) the amount of the resultant force in y-direction applied on the interior boundary or on the exterior boundary will be $2\pi(\kappa+1)F$. The relevant loading condition is shown in Figure 6(b).

For the mentioned loading case, computations for five cases, $a=\lambda_1-0.00002$, $a=\lambda_1$, $a=\lambda_1+0.00002$, $a=0.9\lambda_1$, and $a=1.1\lambda_1$ ($\lambda_1=1.60640$) are performed. The computed results for $f_x(\theta)$, $f_y(\theta)$, $g_x(\theta)$ and $g_y(\theta)$ are plotted in Figures 13–18. For comparison, the exact results from Equations (34) and (35) are also shown in the figures.

The most significant feature of the degenerate scale problem can be seen from Figures 15 and 16. In fact, the exact values for $f_y(\theta)$ are varying within the ranges $0.091\leqslant f_y(\theta)\leqslant 1.091$ (see Figure 16). However, if $a=\lambda_1$ is adopted, we have $f_y(\theta)|_{\theta=12^\circ}=128.871$. Therefore, if the critical value $a=\lambda_1$ is adopted, the BIE shown by Equation (8) cannot give a correct result. In addition, if $a=0.9\lambda_1$ or $a=1.1\lambda_1$ is adopted, the error for $f_y(\theta)$ from the exact solution is very small and this situation can be seen from Figure 16. From Figures 13, 14, 17 and 18, it is seen that the dependence of the functions $f_x(\theta)$, $g_x(\theta)$ and $g_y(\theta)$ to the used size is not significant. It is interesting to point out that only the function $f_y(\theta)$ (i.e. the p_2 component along the exterior boundary) has a unstable numerical result when $a\approx\lambda_1$ (refer to Figure 15).

For the mentioned loading case, computations are also made for five cases, $a=\lambda_2-0.00002$, $a=\lambda_2$, $a=\lambda_2+0.00002$, $a=0.9\lambda_2$, and $a=1.1\lambda_2$ ($\lambda_2=1.93321$) are performed. In this computation, no wrong results have been found.

The situation in the second example is similar to the case discussed in the problem of the annular region. From the above-mentioned results shown by Figures 13–18, the following property

DOI: 10.1002/nme

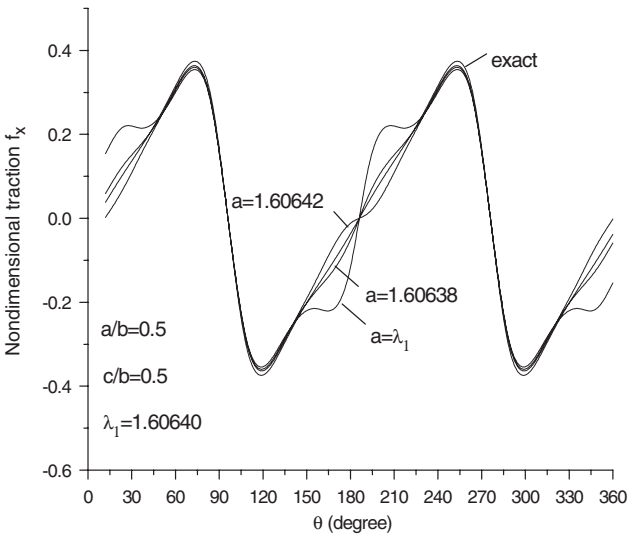

Figure 13. Non-dimensional boundary tractions $f_x(\theta)$ on the exterior boundary in the second example, for $a=\lambda_1-\varepsilon$, $a=\lambda_2$ and $a=\lambda_1+\varepsilon$ cases ($\lambda_1=1.60640$, $\varepsilon=0.00002$) under the condition $b/a=0.5$ and $c/a=0.5$ (see Figures 1, 6(b) and Equation (31)).

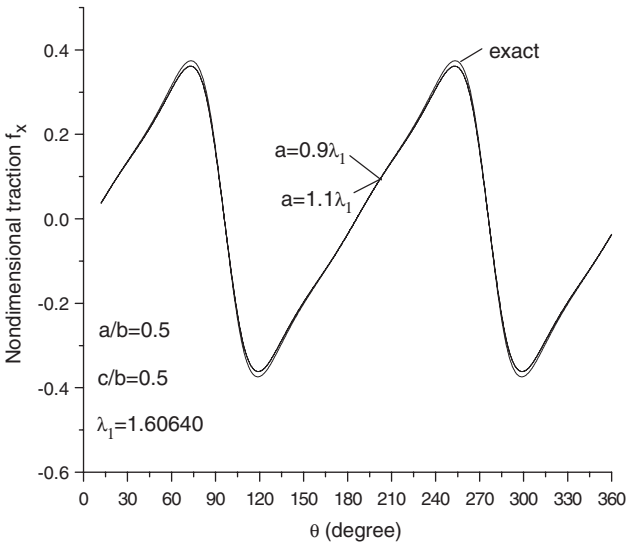

Figure 14. Non-dimensional boundary tractions $f_x(\theta)$ on the exterior boundary in the second example, for $a=0.9\lambda_1$ and $a=1.1\lambda_1$ cases ($\lambda_1=1.60640$) under the condition $b/a=0.5$ and $c/a=0.5$ (see Figures 1, 6(b) and Equation (31)).

may be found. If the condition $a=\lambda_1$ is satisfied, $p_1=0$, $p_2=g_0$ (g_0—any constant value) (for $(x(x_1,x_2)\in B_0)$) and $p_1=0$, $p_2=0$ (for $(x(x_1,x_2)\in B_1)$) is a non-trivial solution for the homogeneous integral equation (9).

DOI: 10.1002/nme

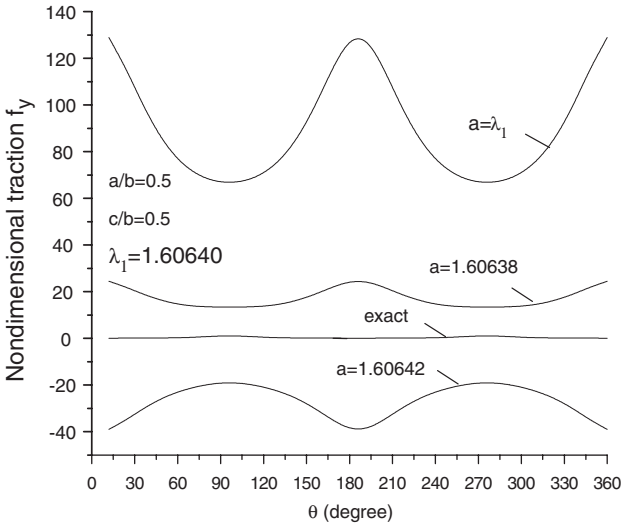

Figure 15. Non-dimensional boundary tractions $f_y(\theta)$ on the exterior boundary in the second example, for $a = \lambda_1 - \varepsilon$, $a = \lambda_2$ and $a = \lambda_1 + \varepsilon$ cases ($\lambda_1 = 1.60640$, $\varepsilon = 0.00002$) under the condition $b/a = 0.5$ and $c/a = 0.5$ (see Figures 1, 6(b) and Equation (31)).

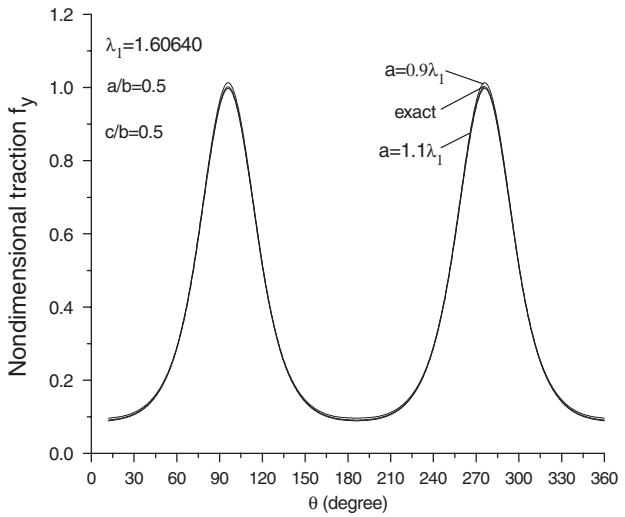

Figure 16. Non-dimensional boundary tractions $f_y(\theta)$ on the exterior boundary in the second example, for $a = 0.9\lambda_1$ and $a = 1.1\lambda_1$ cases ($\lambda_1 = 1.60640$) under the condition $b/a = 0.5$ and $c/a = 0.5$ (see Figures 1, 6(b) and Equation (31)).

From the above-mentioned results we see if the adopted size differs from the critical value for the degenerate scale by a rather small value, for example, 0.00002 ($= 0.0013\%$ of the critical value), the computed results are incorrect. Meantime, if the adopted size differs from the critical value by

DOI: 10.1002/nme

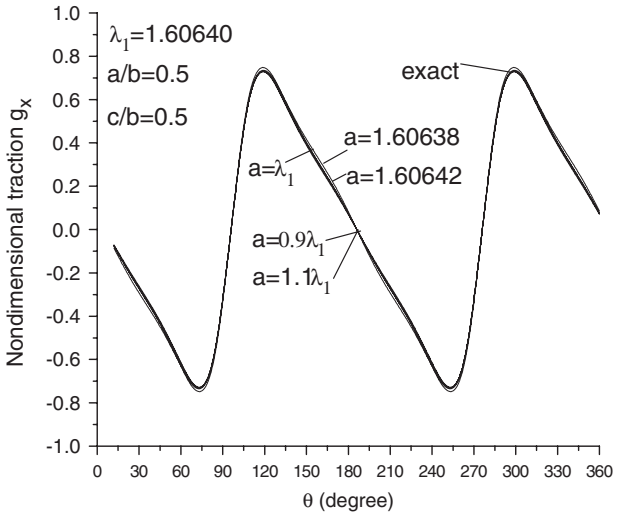

Figure 17. Non-dimensional boundary tractions $g_x(\theta)$ on the interior boundary in the second example, for $a=\lambda_1-\varepsilon$, $a=\lambda_2$, $a=\lambda_1+\varepsilon$, $a=0.9\lambda_1$ and $a=1.1\lambda_1$ cases ($\lambda_1=1.60640$, $\varepsilon=0.00002$) under the condition $b/a=0.5$ and $c/a=0.5$ (see Figures 1, 6(b) and Equation (32)).

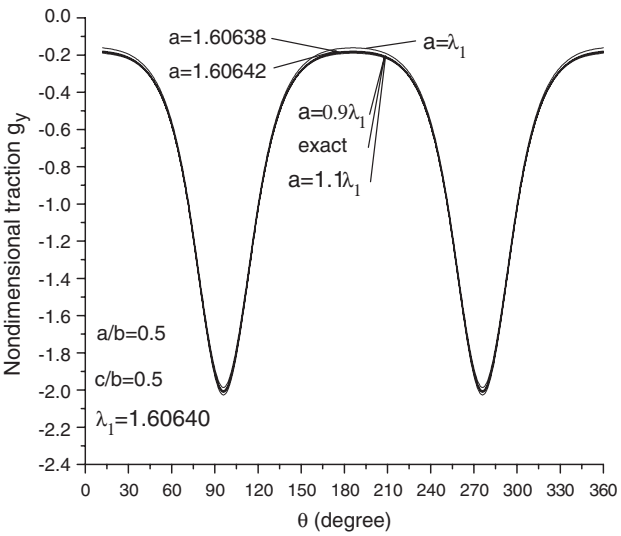

Figure 18. Non-dimensional boundary tractions $g_y(\theta)$ on the interior boundary in the second example, for $a=\lambda_1-\varepsilon$, $a=\lambda_2$, $a=\lambda_1+\varepsilon$, $a=0.9\lambda_1$ and $a=1.1\lambda_1$ cases ($\lambda_1=1.60640$, $\varepsilon=0.00002$) under the condition $b/a=0.5$ and $c/a=0.5$ (see Figures 1, 6(b) and Equation (32)).

more than 10%, the computed results coincide with those from the exact solution. That is to say, if the adopted size is higher (or less) by 10% than the critical value, the adopted size becomes a normal size. In computation, the double precisions are used and the two elliptic boundaries are divided into 120 divisions.

DOI: 10.1002/nme

4. TWO TECHNIQUES FOR AVOIDING THE IMPROPER SOLUTIONS

In this section, two techniques for avoiding the improper solutions are introduced. In the first technique, one must not use the dimension 'a' too near to the two critical values $a=\lambda_1$ and $a=\lambda_2$. It is suggested to use $a\leqslant 0.9\lambda_1$ or $a\geqslant 1.1\lambda_2$. Validity of this approach is easily seen from the computed results in two previously mentioned examples, particularly, from Figures 7, 8, 15 and 16.

From the above-mentioned technique, it is seen that in order to avoid the improper solution, one must evaluate two critical values beforehand. However, this is not a serious problem in computation. Though the exact value of the critical value can only be evaluated from a detailed computation, the range of the critical value can be known from some previous references. For example, for the elliptic ring case ($0.1\leqslant b/a\leqslant 1$), the highest critical value is 3.01622 and the lowest is 1.32168 as listed in Table I. In two-dimensional Laplace equation case, the critical value is equal to one [12]. In this case, if one meets a computation with the size $a=2\,\mathrm{m}$, one simply replaces the dimension $a=2\,\mathrm{m}$ by $a=200\,\mathrm{cm}$, and the numerical instability in the BIE solution disappears. In this case, one does not need to perform a computation for the critical value. This idea was suggested previously [12]. It is suggested that in the case of the slender ratio of configuration less than 0.1, the size $a=100$ is a suitable value to avoid the improper solution.

One may rely upon second technique by changing the form of the kernel $U_{ij}^{*}(\xi, x)$ shown by Equation (3). It is known that the displacement fields for a given stress state can be different from each other by a rigid translation, the theoretical background of the suggested modification is seen. It is convenient to describe this technique in the annular region case discussed in Section 2.3. In the second technique, instead of using $U_{ij}^{*}(\xi, x)$ the following kernel is introduced:

$$U_{ij}^{*1}(\xi, x)=H\{(3-4\nu)\ln(r)\delta_{ij}-r_{,i}r_{,j}+0.5(p+1)\delta_{ij}\}\quad \text{with } H=\frac{-1}{8\pi(1-\nu)G} \tag{36}$$

where 'p' is a constant. Since the kernel $U_{ij}^{*1}(\xi, x)$ is different from $U_{ij}^{*}(\xi, x)$ by a constant, the relevant integrations mentioned in Equation (10) are easy to perform. In this case, the term $[2(3-4\nu)\ln a-1]$ (if using the kernel $U_{ij}^{*}(\xi, x)$) in Equations (11) and (12) will be changed into $[2(3-4\nu)\ln a+p]$ (if using the kernel $U_{ij}^{*1}(\xi, x)$). Similarly, the critical value is determined by

$$2(3-4\nu)\ln a+p=0 \tag{37}$$

The solution of Equation (37) is found to be

$$a=\gamma_{\mathrm{d}},\quad \text{where } \gamma_{\mathrm{d}}=\exp[-p/2(3-4\nu)] \tag{38}$$

Particularly, several of them are listed below

$$a=\gamma_{\mathrm{d}},\quad \text{where } \gamma_{\mathrm{d}}=\exp[1/2(3-4\nu)]=1.32019\quad (p=-1) \tag{39a}$$

$$a=\gamma_{\mathrm{d}},\quad \text{where } \gamma_{\mathrm{d}}=\exp[0]=1\quad (p=0) \tag{39b}$$

DOI: 10.1002/nme

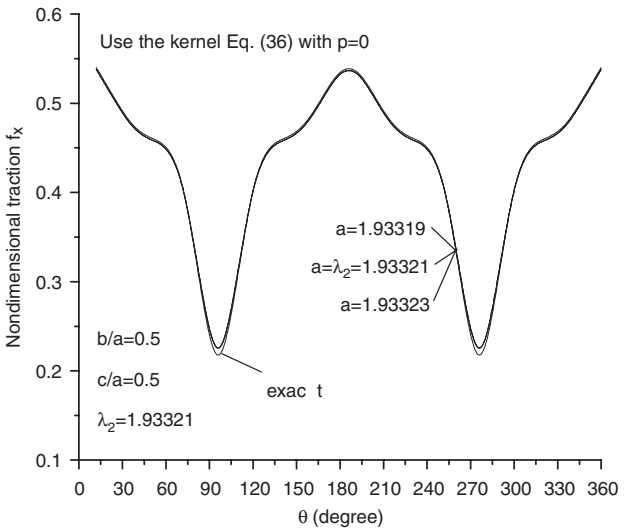

Figure 19. Non-dimensional boundary tractions $f_x(\theta)$ on the exterior boundary in the first example using the kernel shown by Equation (36) with $p=0$, for the $a=\lambda_2-\varepsilon$, $a=\lambda_2$ and $a=\lambda_2+\varepsilon$ cases ($\lambda_2=1.93321, \varepsilon=0.00002$) under the condition $b/a=0.5$ and $c/a=0.5$ (see Figures 1, 6(a) and Equation (31)).

$$a=\gamma_{\mathrm{d}}, \quad \text{where } \gamma_{\mathrm{d}}=\exp[-1/2(3-4\nu)]=0.75747 \quad (p=1) \tag{39c}$$

$$a=\gamma_{\mathrm{d}}, \quad \text{where } \gamma_{\mathrm{d}}=\exp[-2/2(3-4\nu)]=0.57375 \quad (p=2) \tag{39d}$$

From listed results, it is seen that if 'p' takes positive value, the critical value will be considerably reduced. Also, the $p=-1$ corresponds to the case of using the kernel $U_{ij}^{*}(\xi, x)$.

Clearly, the mentioned behaviour is also valid for the case of ellipse-shaped ring region. For the stress field defined by Equation (28), we make the similar computation under the condition of using the kernel $U_{ij}^{*1}(\xi, x)$ with $p=0$. The conditions $b/a=0.5$ and $c/a=0.5$ are still used. The computed results for $f_x(\theta)$ for three cases, $a=1.93319$, $a=\lambda_2=1.93321$ and $a=1.93323$, are plotted in Figure 19. From computed results in Figure 19, we see that the second technique provides sufficient accurate result. Note that Figure 7 is computed under the same geometrical conditions, and only the used kernel is different (by using the kernel $U_{ij}^{*}(\xi, x)$ shown by Equation (3)). After comparing the results in Figures 7 and 19, the efficiency of the second technique is proved. This technique was suggested previously [12, 15].

5. CONCLUSIONS

Numerical computation and examination are highlighted in this paper. In fact, the merit of the degenerate scale problem is to find the critical value for the degenerate scale, which is defined by Equation (9). After discretization, the homogeneous algebraic equation (18) can be deduced from Equation (9). In an earlier stage of this study, the authors were aware of result proposed in [8].

DOI: 10.1002/nme

Paper [8] suggested the number of the critical value was one (refer to Equation (24)). Later, the property of the function $g(a)$ ($g(a) = \det(\mathbf{U})/h(a_1)$ proportional to $\det(\mathbf{U})$) is examined by us. Figure 4 is a typical result of the numerical examination where two roots for the equation $g(a) = 0$ are clearly indicated. Clearly, this finding is not easy to obtain by pure mathematical analysis.

Secondly, after numerical examination one can know the characters of solutions in more detail. For example, not all the traction components are unstable in computation when the critical value of the degenerate scale is approaching. It was shown in first numerical example that only the function $f_x(\theta)$ (i.e. the p_1 component along the exterior boundary) has a unstable numerical result when $a \approx \lambda_2$ (refer to Figure 7).

Two techniques for avoiding the improper solutions are suggested. It is proved that the suggested techniques can give accurate results for the problem.

APPENDIX: EVALUATION OF ONE TERM IN EQUATION (11)

From Equation (10), the investigated integral (a portion of Equation (10)) takes the form

$$J_{1a} = \int_{B_1} (U_{11}^*(\xi, x) p_1(x) + U_{12}^*(\xi, x) p_2(x)) \, \mathrm{d}s(x) \quad (\text{for } \xi = a \exp(\mathrm{i}\beta_0) \in B_0) \tag{A1}$$

where

$$U_{ij}^*(\xi, x) = H\{(3 - 4v) \ln r \delta_{ij} - r_{,i} r_{,j}\} \tag{A2}$$

Substituting $p_1 = g_1$ and $p_2 = 0$ into Equation (A1) yields

$$J_{1a} = g_1 \int_{B_1} U_{11}^*(\xi, x) \, \mathrm{d}s(x) \quad (\text{for } \xi = a \exp(\mathrm{i}\beta_0) \in B_0) \tag{A3}$$

where

$$U_{11}^*(\xi, x) = H\{(3 - 4v) \ln r - r_{,1} r_{,1}\} \tag{A4}$$

Substituting Equation (A4) into (A3), we have

$$J_{1a} = H g_1 (K_{1a} - K_{1b}) \tag{A5}$$

where

$$K_{1a} = (3 - 4v) \int_{B_1} \ln r \, \mathrm{d}s(x) \quad (\text{for } \xi = a \exp(\mathrm{i}\beta_0) \in B_0) \tag{A6}$$

$$K_{1b} = \int_{B_1} r_{,1} r_{,1} \, \mathrm{d}s(x) \quad (\text{for } \xi = a \exp(\mathrm{i}\beta_0) \in B_0) \tag{A7}$$

The derivation for the integral K_{1b} is as follows (Figure 2). Since the integration is performed on the circle 'B_1', therefore, we can let (here 'z' corresponds to the variable 'x')

$$z = c \exp(\mathrm{i}\theta), \quad \mathrm{d}z = \mathrm{i}c \exp(\mathrm{i}\theta) \, \mathrm{d}\theta, \quad \mathrm{d}\theta = \frac{\mathrm{d}z}{\mathrm{i}z}, \quad \overline{z} = c^2/z, \quad \mathrm{d}s = c \, \mathrm{d}\theta \tag{A8}$$

DOI: 10.1002/nme

Secondly, for vector $\boldsymbol{\xi z}$ and its projection (Figure 2) we have

$$r_{,1} = \frac{\overline{CE}}{\overline{CD}}, \quad 2\overline{CE} = (z-\xi) + (\overline{z}-\overline{\xi}) = (z-\xi) + (c^2/z - \overline{\xi})$$
$$\overline{CD}^2 = (z-\xi)(\overline{z}-\overline{\xi}) = (z-\xi)(c^2/z - \overline{\xi}) \tag{A9}$$

After using Equations (A8) and (A9), the K_{1b} can be reduced to

$$K_{1b} = \frac{c}{4}\int_{B_1} \frac{(2\overline{CE})^2}{\overline{CD^2}}\,\mathrm{d}\theta = \frac{c}{4}\oint_{B_1} \frac{[(z-\xi)+(c^2/z-\overline{\xi})]^2}{(z-\xi)(c^2/z-\overline{\xi})}\,\frac{\mathrm{d}z}{\mathrm{i}z} \tag{A10}$$

It is seen that the following integral (proportional to K_{1b}) can be integrated in a closed form [14]

$$L = \frac{1}{2\pi\mathrm{i}}\oint_{B_1} \frac{[(z-\xi)+(c^2/z-\overline{\xi})]^2}{(z-\xi)(c^2/z-\overline{\xi})}\,\frac{\mathrm{d}z}{z-0} \tag{A11}$$

Only if (1) one considers the integrand (the term $[(z-\xi)+(c^2/z-\overline{\xi})]^2/[(z-\xi)(c^2/z-\overline{\xi})]$ in Equation (A11)) as an analytic function outside the region 'B_1', (2) one separates the singular portion of the integrand and (3) one uses the generalized residue theorem in complex variable theory [14]. Finally, after some manipulations, one obtains

$$K_{1b} = c\pi(1 + \cos 2\beta_0 - \delta^2 \cos 2\beta_0) \quad (\text{where } \delta = c/a) \tag{A12}$$

The integral K_{1a} can be evaluated in a similar way. For the sake of compactness, the relevant derivation is omitted here.

ACKNOWLEDGEMENTS

The project was supported by the National Natural Science Foundation of China.

REFERENCES

1. Rizzo FJ. An integral equation approach to boundary value problems in classical elastostatics. *Quarterly Journal of Applied Mathematics* 1967; **25**:83–95.
2. Cruse TA. Numerical solutions in three-dimensional elastostatics. *International Journal of Solids and Structures* 1969; **5**:1259–1274.
3. Brebbia CA, Tells JCF, Wrobel LC. *Boundary Element Techniques—Theory and Application in Engineering*. Springer: Heidelberg, 1984.
4. Jaswon MA. Integral equation methods in potential theory. I. *Proceedings of the Royal Society, Series A* 1963; **275**:23–32.
5. Power H, Wrobel LC. *Boundary Element Methods in Fluid Mechanics*. Computational Mechanics Publications: Southampton, 1995.
6. Cheng AHD, Cheng DS. Heritage and early history of the boundary element method. *Engineering Analysis with Boundary Elements* 2005; **29**:286–302.
7. He WJ, Ding HJ, Hu HC. Non-equivalence of the conventional boundary integral formulation and its elimination for plane elasticity problems. *Computers and Structures* 1996; **59**:1059–1062.
8. He WJ, Ding HJ, Hu HC. Degenerate scales and boundary element analysis of two dimensional potential and elasticity problems. *Computers and Structures* 1996; **60**:155–158.
9. Chen JT, Kuo SR, Lin JH. Analytical study and numerical experiments for degenerate scale problems in the boundary element method of two-dimensional elasticity. *International Journal for Numerical Methods in Engineering* 2002; **54**:1669–1681.

DOI: 10.1002/nme

10. Chen JT, Lin JH, Kuo SR, Chiu YP. Analytical study and numerical experiments for degenerate scale problems in boundary element method using degenerate kernels and circulants. *Engineering Analysis with Boundary Elements* 2001; **25**:819–828.
11. Chen JT, Lee CF, Chen IL, Lin JH. An alternative method for degenerate scale problems in boundary element methods for the two-dimensional Laplace equation. *Engineering Analysis with Boundary Elements* 2002; **26**: 559–569.
12. Chen JT, Lin SR, Chen KH. Degenerate scale problem when solving Laplace's equation by BEM and its treatment. *International Journal for Numerical Methods in Engineering* 2005; **62**:233–261.
13. Chen JT, Shen WC. Degenerate scale for multiply connected Laplace equation. *Mechanics Research Communication* 2007; **34**:69–77.
14. Muskhelishvili NI. *Some Basic Problems of Mathematical Theory of Elasticity*. Noordhoof: Netherlands, 1953.
15. Telles JCF, Paula FA. Boundary element with equilibrium satisfaction? A consistent formulation for potential and elastostatic problems. *International Journal for Numerical Methods in Engineering* 1991; **32**:609–621.

DOI: 10.1002/nme